

Comparison Between Simulations of Real and Ideal LRE Combustion of $\text{LO}_2\text{-CH}_4$

A. Minotti* and C. Bruno*

Department of Mechanics and Aeronautics, University of Rome "La Sapienza", Via Eudossiana 18, 00184, Rome, Italy

Abstract: This work is a contribution toward better understanding of the impact of real gas behaviour on injection, mixing and combustion in future Liquid Rocket Engines. Recent US and EU patents indicate that work is already underway in this key area, and is suggestive of potential breakthroughs in injector design. To this purpose, three simulations of coaxial LO_2/CH_4 Liquid Rocket Engines injector flames at supercritical conditions and at 1.18 equivalence ratio are presented. Real and ideal gas properties are used to investigate differences. Properties have been calculated or are from experiments, and are fitted by 6th order polynomials and introduced in the computational software. An Eddy Dissipation Model describes the turbulence-chemical kinetics coupling. Two of the three simulations are carried out at 15MPa. Two of them assume real gas properties while the other assumes ideal gas behaviour. The O_2 and CH_4 injection temperature is assumed supercritical. Simulations performed predict that, due to compressibility, pressure is not uniform inside the combustion chamber; therefore one more simulation was carried out using real gas properties at the highest pressure found inside the combustion chamber, i.e. at 16.5MPa. Because the Reynolds numbers of the real gas are lower than those for ideal gas, the real gas potential core lengths are predicted longer than in the ideal case, while maximum temperatures are substantially lower due to the different specific heats behaviour. These results show that using real gas properties as accurately as possible is a key issue in the preliminary design of LRE injectors and combustion chambers, and may lead to innovative new cryogenic injectors and in the future new patents.

Keywords: Supercritical conditions, $\text{LO}_2\text{-CH}_4$ liquid rocket engines, combustion, thermophysical properties.

INTRODUCTION

Raising performance and reducing cost of future Liquid Rocket Engines (LRE) require combustion chamber pressure often higher than the propellants critical pressure, and often higher than that of the products; this is not necessarily true for the injection temperature, which is usually lower than the critical temperature of oxygen but higher than that of the fuel. Cost reduction is of much interest in Europe, where kerosene and liquid methane, posing fewer technology and logistic problems than liquid hydrogen, are candidate fuels for future main and booster LRE [1-5]. The physics of supercritical flows is relatively unexplored, and LRE manufacturers are trying to take advantage of what is known in designing injection systems. Their major advantage, and the subject of patents as well [6, 7], is the theoretical absence of a liquid phase thus of vaporization, this lasts a slow process that controls combustion times [8-10] and therefore chamber length and combustion efficiency. Hence moving from conventional to supercritical injection of propellants in a rocket chamber will simplify both operation and design of injector components, since there will not be a liquid to atomize.

At this stage of our knowledge it is still unclear what happens when propellants are injected supercritically, namely whether flash vaporization takes place, or they actually gasify inside the injectors and emerge inside the chamber as gaseous jets.

It is for these reasons that the scant information available is essentially proprietary and can sometimes be gleaned only by a patent search. It must be said that only two patents [6, 7] on this aspect of LRE have been found by these authors. Until information became recently available, a commonplace assumption in designing LRE is to consider the gas as ideal even at high [i.e., supercritical] pressure. To check how good this assumption is, work done by these authors has investigated differences between real and ideal gas behaviour in LO_2/CH_4 flames [11].

That work has shown that assuming ideal gas behaviour (i.e., compressibility factor $Z=1$) at transcritical conditions leads to large errors: at high pressure and at typical LRE injection conditions the compressibility factor Z is less than unity, and transport and thermodynamics properties are complex functions of two variables (P and T) for each species.

That is especially true close to their critical point, leading to significant effects on mass, momentum and energy exchange during combustion.

In this context, the purpose of this article is not to design new injectors, although that will naturally be enabled by better understanding of their supercritical physics, but to investigate:

- 1) The differences in LRE design parameters (maximum temperature, pressure and potential core length of coaxial injectors) obtained using ideal and real gas properties;

*Address correspondence to these authors at the Department of Mechanics and Aeronautics, University of Rome "La Sapienza", Via Eudossiana 18, 00184, Rome, Italy; Tel: +39 06 44585-280; Fax: +39 06 488-1759; E-mails: angelo.minotti@uniroma1.it, Claudio.Bruno@uniroma1.it

- 2) Whether thermophysical properties must be described as local functions of T and P, or they can be described as function of T only and at a fixed [design] pressure. This that is possible, it would reduce implementation in CFD codes and CPU times, while maintaining physical accuracy. This second question bears on LRE operation as well as on its simulation.

Accordingly, three reacting LO₂/CH₄ simulations of a generic coaxial LRE injector, were carried out, see Table 1, and their results are discussed in the next sections. Predicting mixing and combustion downstream of a single coaxial injector element is of primary importance because, for almost all of the injector *near* region, each injector operates independently of others, and the general picture of the overall reacting flowfield in a LRE may be interpreted as a *collection* of many coaxial injector flames.

Table 1. Simulations: Input Data

Simulation	Design Pressure	Properties Prediction Pressure	Injection Temperature		Gas Model
			CH ₄	O ₂	
1 st -Supercritical	15MPa	15MPa	300K	300K	real
2 nd - Supercritical	15MPa	15MPa	300K	300K	ideal
3 rd - Supercritical	15MPa	16.5MPa	300K	300K	real

From Table 1, two pressures are assumed (15MPa, 16.5MPa); this because real gas properties are function not only of temperature (as in ideal gases) but also of pressure [12]. The CFD code used in these simulations (FLUENT 6.2.16) cannot accept properties as functions of temperature and pressure simultaneously, so the following strategy has been implemented: besides those at the *nominal* P=15MPa, the third simulation was carried out using real gas properties predicted at 16.5MPa, the *highest* pressures found in the combustion chamber at the *nominal* pressure of 15MPa. In this way it was hoped to bracket LRE combustion behaviour due to the effect of pressure on real gas physics.

Table 2 reports the critical conditions of the four species assumed in the present reacting simulations.

Table 2. Critical Properties of Species Assumed of Interest to LO₂/CH₄ LRE

	T _c [K]	P _c [atm]
O ₂	154.6	49.8
CO ₂	304.2	72.8
H ₂ O	647.3	217.6
CH ₄	190.4	46

In literature there are some examples of simulations of non reacting and reacting flows at subcritical and supercritical conditions, but most of them are for LOx/H₂ propellants: see, for instance, Chehroudi [13,14], Mayer and Tamura [15-18], Oefelein and Yang [19-23] and O’Kongo, Harstad, and Bellan [24,25]. Only recent experimental [26,27] and numerical [28] papers on LOx/CH₄ mixtures at transcritical conditions have

appeared. Among the most recent works are those of Ruiz [29] and De Giorgi [30] The first analysis is a 3-D non reactive flow with LES using 5.5M cells; the most important result is the transcritical-supercritical potential core length comparison. It shows that in the supercritical regime the potential core length is shorter than that transcritical. Our work (below) shows that the result is due to the different Reynolds numbers, and in particular to the different viscosities at the two inlet conditions (keeping the mass flow inlet fixed, the Reynolds number is a function only the viscosity). The second work deals with a reactive flow of LOX and CH₄ at 150 atm and compares the effects of assuming ideal and real properties using the Peng-Robinson real gas equation. Because results are obtained for fixed inlet velocity (not fixed mass flow rates, as done in the present work), the heat release changes and affects the comparison.

This field is still evolving, and more information on the differences between the two regimes will certainly become available in the future. In contrast, experimental data for reactive flows would be more than welcome, but seem still a long way off because of the forbidding LRE environment.

MODELLING DETAILS

A summary of the three simulations of LO₂/CH₄ axisymmetric coaxial jets combustion is presented. All use the same geometry (see Fig. 3), computational mesh (512000 cells) and boundary conditions: mass flow imposed at inlet, constant temperature on the walls except for the post tip, which is adiabatic and constant pressure at the outlet.

The CH₄ and O₂ jets are supercritical. Simulations were carried out using steady state Favre-averaged Navier-Stokes (FANS) equations; turbulence was modelled by a k-ε model. Real properties have been described by means of 6th order polynomial fits [11] as function of temperature and calculated at the pressure values reported in Table 1.

These polynomials are based on:

1. Experimental data (from NIST tables [31]), where possible, and data obtained with the Lee-Kesler [32] equation of state (EOS), for what concerns density and Cp. The choice of the EOS based on L-K²² is the result of a comparison between the EOS by Lee-Kesler [32], Soave [33], Redlich-Kwong [34] and Peng-Robinson [35] made in [12, 36] and of the analysis of Harstad *et al.* [37]. The comparison indicated the Lee-Kesler EOS fits the NIST data [11, 37] (especially in the lower and upper range) better than all other EOS, its penalty being a longer computational time. Fig. (1) provides, among the

thermophysical properties, the methane density behaviour, as function of temperature, with the experimental data and Lee-Kesler data highlighted.

- Experimental data (from NIST), where possible, and data obtained with the Chung *et al.* method [38], for what concerns viscosity and thermal conductivity. The choice of this method is the result of a comparison between this method and that of Ely and Hanley [39] also made in [12, 36]: this comparison indicated that Chung *et al.* fits the NIST [11, 31] data better. Fig. (2) provides, among the transport properties, the methane viscosity behaviour, as function of temperature, with the experimental data and Chung *et al.* data highlighted.

The polynomial fits have been introduced inside a CFD code (FLUENT 6.2.16) and validated [12] by simulating and comparing the experimental results of a single jet of N₂, in a quiescent N₂ chamber, injected both at supercritical temperature and at subcritical temperature [40, 41]. After validation, two LO₂/CH₄ non-reacting coaxial jet simulations, at sub and supercritical conditions, have been carried out [12] and studied [13]. Results as potential core and jet spread angle have been compared with those from Villermaux theory [42, 43] and with those in [44], showing good agreement [12] especially for the simulation performed at subcritical conditions. Villermaux theory has been developed for coaxial water-water jets, much closer to subcritical than to supercritical conditions.

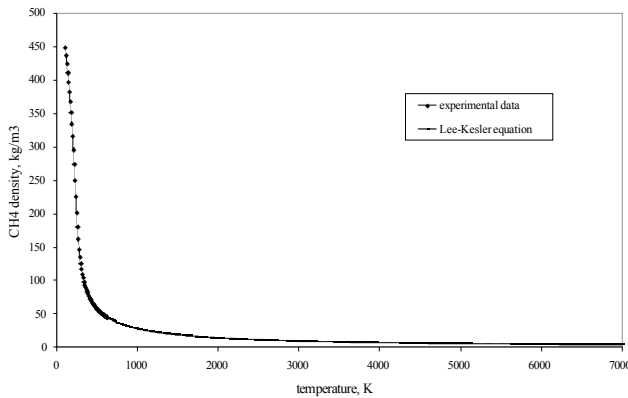


Fig. (1). CH₄ density: experimental data and extrapolation.

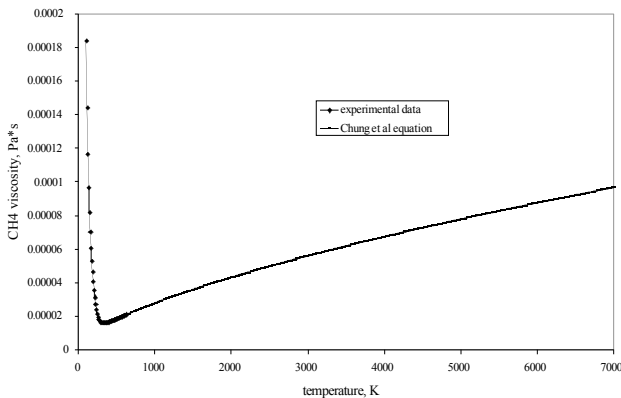


Fig. (2). CH₄ viscosity: experimental data and extrapolation.

The “Ideal” simulation was carried out using the ideal gas equation of state $\frac{P}{\rho RT} = 1$, Cp’s were predicted using the same polynomial fits in CEA 400 [45-48] (introduced in the CFD software using 6th order polynomials [11]) and viscosity and thermal conductivity were calculated using gas kinetic theory (equations 1 and 2) [49, 50]:

$$k_i = \frac{15}{4} \cdot \frac{R}{M_{w_i}} \mu_i \left[\frac{4}{15} \cdot \frac{C_{p_i} M_{w_i}}{R} + \frac{1}{3} \right]; \quad (1)$$

$$\mu_i = 2.6 \times 10^{-6} \frac{\sqrt{M_{w_i} T}}{\Omega_{\mu i} \sigma_i^2}; \quad (2)$$

The last step has been the introduction of one single global reaction, i.e.:



The crude kinetics of (3) overestimates maximum temperature; therefore the heat of reaction was appropriately modified by correcting the methane formation enthalpy, so $\Delta H'_{f\text{CH}_4} = -1.3 \times 10^8$ [J/kmol], see reference 2 for details.

The turbulence-chemistry coupling was modelled by means of an Eddy-Dissipation concept [51-56] in which the source term (R_i) of the i -specie production is:

$$R_i = v'_{i,r} M_{w,i} A \rho \frac{\text{eps}}{K} \min_{\mathfrak{R}} \left(\frac{Y_{\mathfrak{R}}}{v'_{i,r} M_{w,\mathfrak{R}}} \right) \quad (4)$$

where $Y_{\mathfrak{R}} \equiv$ mass fraction of the reactant \mathfrak{R} ; $A \equiv$ empirical constant, 4.0; $\frac{\text{eps}}{K} \equiv$ inverse of turbulent time scale; $v'_{i,r} \equiv$ stoichiometric coefficient of the i -th species.

The key assumption of this model is that chemical times are shorter than those of turbulence, and thus that each reaction rate is controlled by the velocity of turbulent mixing.

This condition was verified by calculating inside the recirculation zone the turbulence time (κ/ϵ), which turned out to be $\approx 10^{-4}$ s, while chemical times for a methane-oxygen reaction are reported in Table 3. Chemical times were separately predicted by simulations with the CHEMKIN code [57] using a CH₄/O₂ perfect stirred reactor detailed reaction mechanism at the same design pressure of the LRE, i.e. 15MPa.

Table 3. Methane-Oxygen Reaction Times as a Function of Temperature at 15MPa

Temperature [K]	Times [s]
1100	3.1×10^{-4}
1300	2×10^{-5}
>1500	$< 1.7 \times 10^{-6}$

Fig. (3) reports a part of the domain and the structured mesh. The oxygen inlet duct thickness is 0.0035m while the methane inlet duct thickness is 0.001m and the post tip is

0.0004m. Inlet ducts length is 0.005m while the entire chamber is 0.105m.

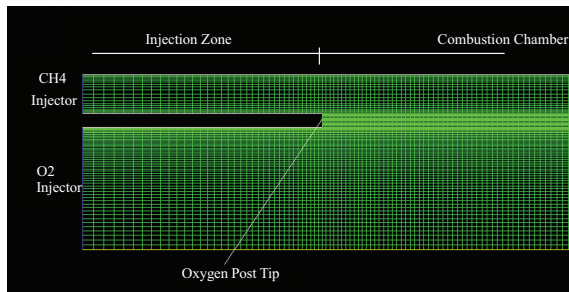


Fig. (3). LO₂/CH₄ schematic diagram of the computational domain.

Fig. (4) provides the wall unit x^+ value at the first point along the oxygen post-tip; this is useful to highlight the level of accuracy obtained [58, 59]. This figure shows that the first point is among 0.02 and 0.7 wall units, and that $\Delta x^+ < 1$, assuring physically realistic grid resolution.

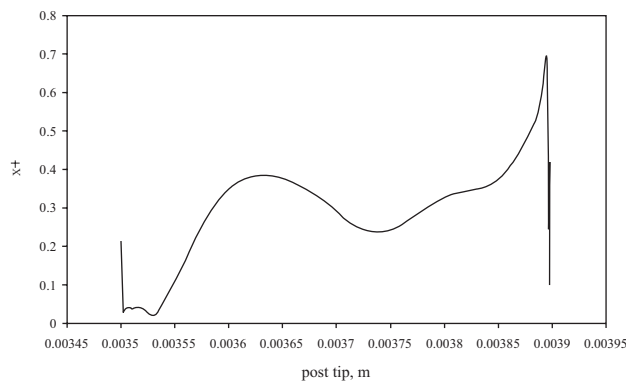


Fig. (4). Post-tip x^+ .

SUPERCRITICAL CH₄ REACTING WITH SUPERCRITICAL O₂: REAL VS IDEAL GAS PROPERTIES RESULTS (SIMULATIONS 1 AND 2)

Simulations 1 and 2 deal with methane and oxygen both injected at supercritical temperature and pressure. Ideal and real gas properties are used and results are compared. Real gas properties were calculated at the nominal design pressure, i.e. 15MPa. Operating conditions are reported in Table 4 for both cases: note values for the compressibility factor Z equal to 0.948 for the oxygen and 0.824 for the methane (in ideal gases Z is equal to 1).

Table 5 reports reactants percentage differences between real and ideal properties i.e. $\frac{((ideal-real)/ideal)*100}$ of reactants: a negative value means that the real property value is greater than the ideal one. The comparison has been carried out by keeping fixed the reactants flow rates at inlet and their injection temperatures, in order to have identical heating values and Reynolds numbers function only of viscosity.

Table 5 shows that differences are important, especially as far as the isobaric specific heats and the Reynolds numbers; in particular real Cp are greater than ideal ones (Figs. 5, 6), while the opposite is true for the Reynolds numbers.

Table 4. Supercritical Case: Input Data, REAL and IDEAL

Properties	REAL	IDEAL
Oxygen Injection Temperature [K]	300	300
Oxygen Density [kg/m ³]	203	192
Oxygen Mass Flow [kg/s]	0.386	0.386
Oxygen Velocity [m/s]	49.4 m/s	52.2
Oxygen Molecular Viscosity [kg/m-s]	2.74×10^{-5}	2.6×10^{-5}
Oxygen Reynolds number	2.52×10^6	3.41×10^6
Oxygen Compressibility Factor, Z	0.94	1
Oxygen Isobaric Specific Heat [J/kg K]	1166.3	918.3
Methane Injection Temperature [K]	300K	300K
Methane Density [kg/m ³]	117	96
Methane Mass Flow [kg/s]	0.114	0.114
Methane Velocity [m/s]	37.6	38.3
Methane Molecular Viscosity [kg/m-s]	1.23×10^{-5}	1.12×10^{-5}
Methane Reynolds number	3.03×10^5	3.31×10^5
Methane Compressibility Factor, Z	0.824	1
Methane Isobaric Specific Heat [J/kg-K]	3379.8	2229.1
Momentum Flux Ratio, $M = \rho_2 v_2^2 / \rho_1 v_1^2$	0.24	0.27

Table 5. Reactants Properties % Differences Between Real and Ideal Behaviour

	O ₂	CH ₄
Velocity	6.2 %	16.97 %
Molecular Viscosity	-33 %	-9.8 %
Density	-5.7 %	-8.3 %
Reynolds number	26.4 %	8.7 %
Isobaric Specific Heat	-27 %	-51 %

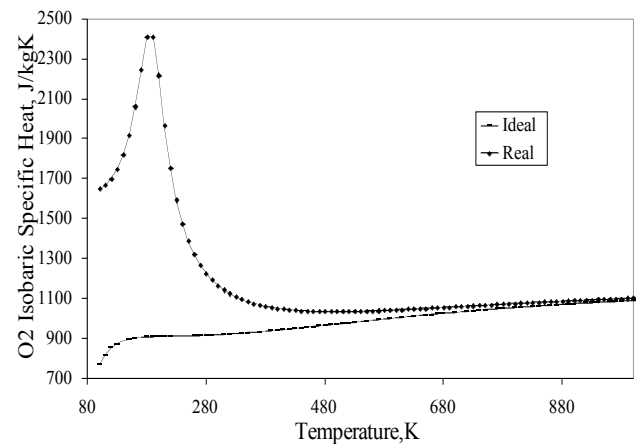


Fig. (5). O₂ ideal and real isobaric specific heat, comparison.

These facts help to understand:

1. the real potential core length is longer than ideal (see Fig. 9 and Table 6); it means that turbulent mixing is enhanced in the ideal case, in fact ideal propellants Reynolds numbers are greater than ideal;
2. the ideal maximum temperature is greater than real (4320K vs 3770K, see Table 6); this result is confirmed also by Figs. (7, 8) which provide the radial temperature at different axial sections for the real and ideal cases.

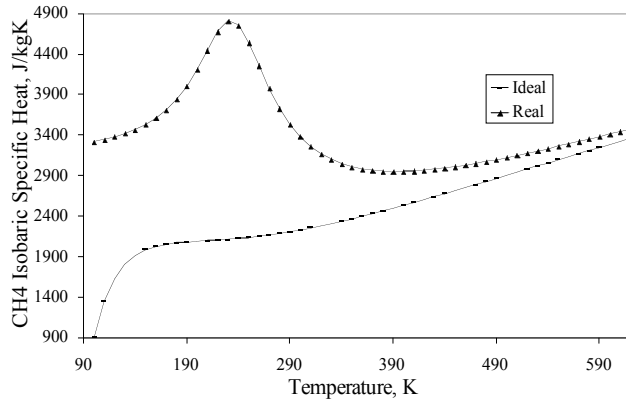


Fig. (6). CH_4 ideal and real isobaric specific heat, comparison.

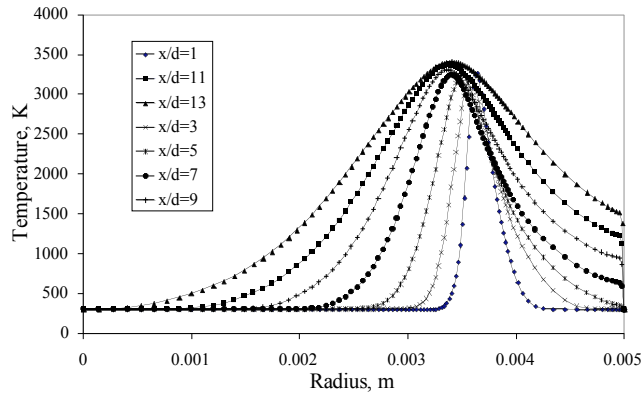


Fig. (7). Real gas: radial temperature at different axial sections.

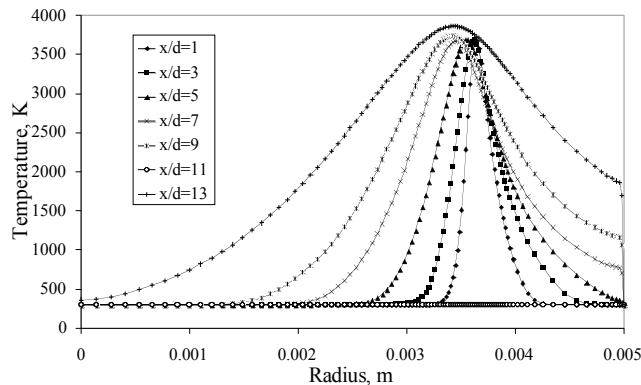


Fig. (8). Ideal gas: radial temperature at different axial sections.

Table 6. Ideal and Real Gas Properties: Results Comparison

	Ideal	Real
Maximum Temperature	4320K	3770K
Oxygen mass fraction at the exit plane	0.915	0.94
Maximum Pressure	16.9MPa	16.4MPa
Jet spreading angle	1.41	1.47

Figs. (9-12) show temperature maps in the ideal and real case; in particular Figs. (9, 11) report a zoom near the post-tip, where the flame anchors, while Figs. (10, 12) provide the entire domain.

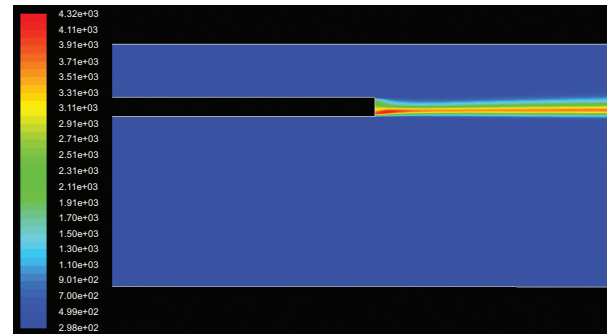


Fig. (9). Ideal Temperature map: zoom near the post tip.

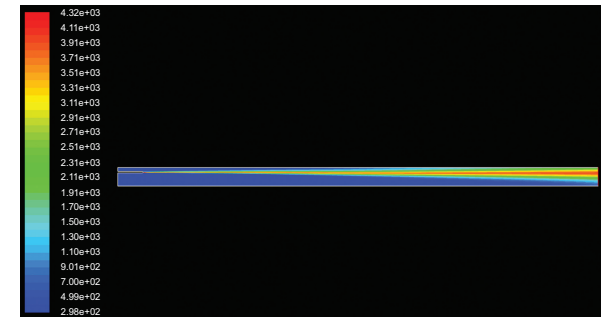


Fig. (10). Ideal Temperature map: entire domain.

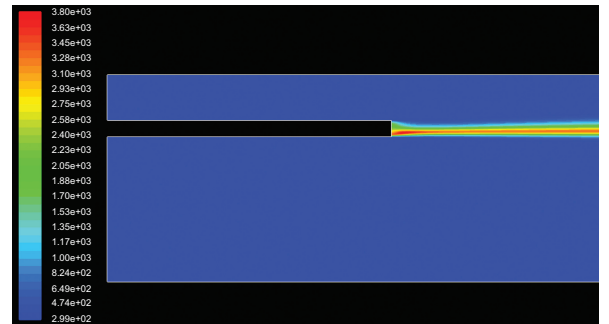


Fig. (11). Real Temperature map: zoom near the post tip.

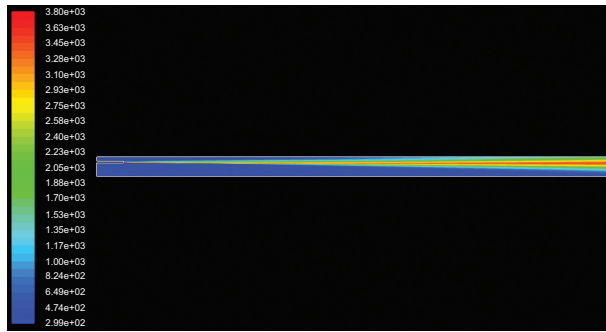


Fig. (12). Real Temperature map: entire domain.

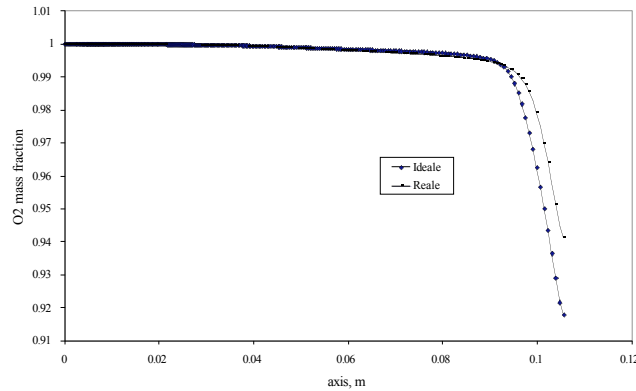


Fig. (13). O₂ axial mass fraction : Ideal gas vs Real gas.

Fig. (13) provides the O₂ real and ideal mass fraction behaviour on the axis and Table 6 reports that values at the exit plane. Table 6 also reports the jet spread angles which are slightly different, i.e. 1.41° (ideal) vs 1.47° (real).

Pressure is not uniform inside the chamber, see Table 6 and Fig. (14) which shows the comparison between Ideal and Real gas axial pressure. Its highest *ideal* value is 16.9MPa (1.9MPa higher than the exhaust pressure), while the *real* one is 16.5MPa (1.5MPa higher than the exhaust pressure and 0.4MPa lower than the maximum value in the ideal case). The reason stays in the higher reactants density at those operating conditions.

Thus, even though the flow is subsonic, there are large pressure differences along the combustion chamber and, at the same time, low velocity and acceleration. This peculiarity obliges us to understand if real gas properties must be defined as punctual function also of Pressure. To investigate this, another simulation has been carried out using real gas properties, calculated at the maximum pressure found inside the chamber, i.e. 16.5MPa; results are in the next section.

SUPERCRITICAL CH₄ REACTING WITH SUPERCRITICAL O₂: REAL GAS PROPERTIES AT 16.5MPa RESULTS (SIMULATION 3)

This simulation repeats the previous real simulation but real gas properties are calculated at the highest pressure found inside the combustion chamber, i.e. 16.5 MPa (see Fig. 14). The goal was to bracket LRE combustion behaviour as function of pressure, since the CFD code used in this work cannot manage properties as function of temperature and

pressure simultaneously. Table 7 reports the operating conditions.

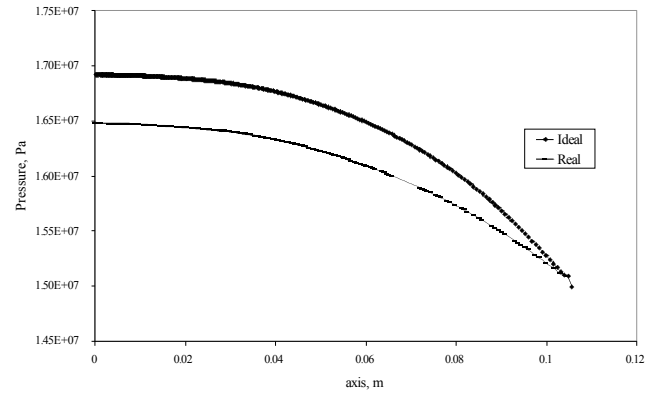


Fig. (14). Axial pressure: Ideal gas vs Real gas.

Table 7. Input Data

	O ₂	CH ₄
Exhaust Pressure [MPa]	15	15
Calculation Pressure of real Gas properties [MPa]	16.5	16.5
Temperature [K]	300	300
Mass flow [kg/s]	0.386	0.114
Velocity [m/s]	44.9	28.8
Molecular Viscosity [kg/m-s]	2.46×10 ⁻⁵	1.72×10 ⁻⁵
Density [kg/m ³]	223.4	129
Reynolds number	2.85×10 ⁶	2.15×10 ⁵
Compressibility Factor, Z	0.949	0.823

Results in Figs. (15-17) show that differences between these two simulations are not significant. Fig. (15) shows a maximum pressure close to 16.4MPa, almost equal to the one reported in Fig. (9). Fig. (16) reports the axial O₂ mass fraction: the difference with the corresponding real simulation prediction at 15MPa (Fig. 14) is slight, 0.938 vs 0.941.

The maximum temperature is close to 3800K (the value obtained with real gas properties at 15MPa was 3770K); Fig. (17) reports the radial temperature at several axial sections. These results support the conclusion that, at least in this supercritical case, it is not really necessary to describe properties as a simultaneous function of temperature and pressure: for engineering purposes it is sufficient to calculate them at the design (nominal) chamber pressure.

CONCLUSIONS

The goal of this study was to investigate the differences in mixing and combustion caused by assuming ideal or real gas properties at supercritical conditions and using a conventional coaxial injector. In this purpose, the test presented consists of a LO₂/CH₄ coaxial injector flame at nominal 15MPa. Three simulations are reported, all assume reactants injected at supercritical temperature and pressure. Of these, the first and the second compare real and ideal gas,

respectively, at 15MPa; the third repeats the first, but using real gas properties calculated at the highest pressure predicted inside the combustion chamber, i.e. 16.5MPa, in order to bracket the LRE supercritical combustion behaviour.

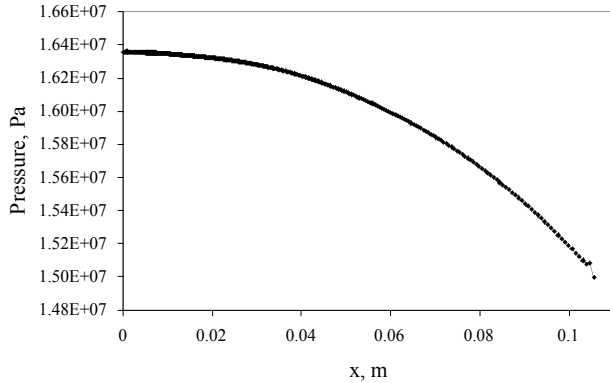


Fig. (15). Real gas, 16.5MPa: axial pressure.

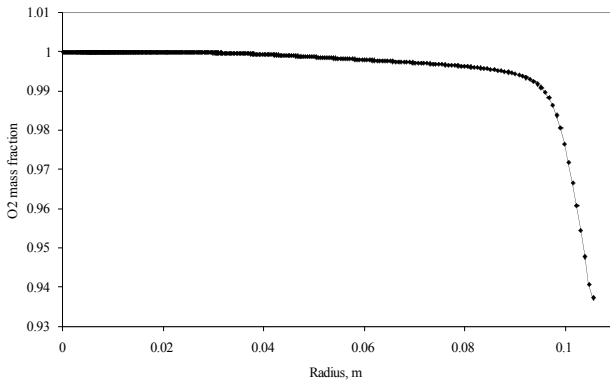


Fig. (16). Real gas, 16.5MPa: axial O_2 mass fraction.

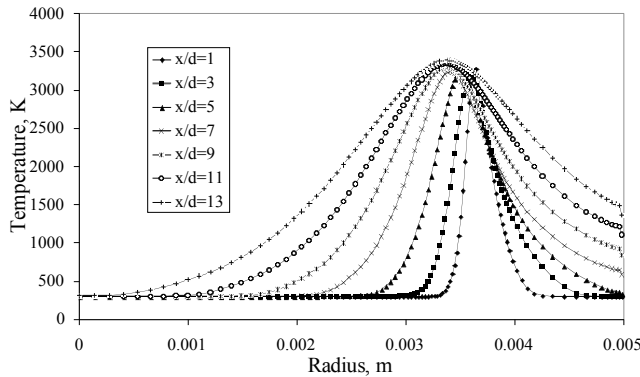


Fig. (17). Real gas, 16.5MPa: Radial temperature at several axial sections.

Ideal and real gas results were compared at fixed propellants mass flow rates, that is, fixed heat release. Thus inlet Reynolds numbers were a function only of viscosity.

Results emphasize the large impact of the simple ideal gas assumption on T and P predictions. This assumption affects simulations from their very start, by changing significantly the nominal inlet parameters. In turn, they influence turbulence, mixing and eventually the entire combustion behaviour. Pressure is not uniform in the

combustion chamber: this is the effect of the enhanced compressibility at supercritical pressure. The resulting higher density yields lower flowfield acceleration., so a third simulation was performed to check how much this non-uniformity affects the original assumption of constant nominal pressure inside the combustion chamber and to LRE combustion behaviour.

Results show that, at supercritical conditions, predictions can be carried out using properties calculated at the nominal design chamber pressure. This is not valid at subcritical conditions [12].

The most important outcome is that ideal gas simulation predicts consistently higher temperatures than in the corresponding real case. This result is justified by the differences between ideal and real C_p close to the critical temperature. Viscosity differences affect Reynolds numbers, therefore affecting mixing and consequently the jets potential core lengths: the higher “ideal gas” Reynolds number (higher mixing) leads to a shorter potential core length and suggests alternative injector designs.

In extreme synthesis, these results indicate that using ideal gas properties in simulations where the compressibility factor is less than 1 will lead to large differences in predictions. These differences are even higher at subcritical inlet conditions because Z is much less [12]. Thus using real gas properties as accurate as possible is a key issue in LRE design, and may lead in a relative near future to novel injection systems for cryogenic combustor chambers.

NOMENCLATURE

- R = Universal gas constant;
- M_w = Molecular weight;
- K = Turbulent kinetic energy;
- ϵ = $\frac{K}{t}$ = turbulent kinetic energy dissipation;
- ν = Stoichiometric coefficient;
- k = Thermal conductivity;
- μ = Molecular viscosity;
- Ω_μ = Collision integral;
- T^* = Reference temperature, $T^* = \frac{T}{(\epsilon/k_B)}$
- σ = Lennard-Jones parameter, finite distance at which inter-particle potential is zero;
- ϵ/k_B = Lennard-Jones parameter, depth of the potential well
- C_p = Isobaric specific heat;
- X = Molar fraction;
- Y = Mass fraction;
- η = Kolmogorov scale.
- x^+ = Wall unit = $\frac{\rho \cdot x \cdot u_\tau}{\mu}$
- u_τ = Friction velocity = $\sqrt{\frac{\mu}{\rho} \frac{\partial v}{\partial x}}$

REFERENCES

- [1] Kalmykov GP, Mossolov SV. Liquid rocket engines working on oxygen+methane for space transportation systems of the XXI century (on the results of scientific and experimental studies). 51th International Astronautical Congress, IAF-00-S.2.10, Rio de Janeiro, Brazil October 2000.
- [2] Burkardt H, Sippel M, Herbertz A, Klevansky J. *Effects of the choice between kerosene and methane on size and performance of reusable liquid booster stages*. 39th Joint Propulsion Conference and Exhibit, AIAA 2003-3122, Huntsville, Alabama July 2003.
- [3] Pempie P, Frohlich T, Vernin H. *LO₂-Methane and Lox-Kerosene high thrust engine trade-off*. 37th Joint Propulsion Conference, AIAA 2001-3542, Salt Lake City, Utah July 2001.
- [4] Klepikov IA, Katargin BI, Chvanov VK. *The new generation of rocket engines, operating by ecologically safe propellant liquid oxygen and liquefied natural gas (methane)*. 48th International Astronautical Congress, IAF-97-S.1.03, Turin 1997.
- [5] Gotz A, Mading C, Brummer L, Haesker D. *Application of non-toxic propellants for future advanced launch vehicles*. 37th Joint Propulsion Conference, AIAA-2001-3546, Salt Lake City, UT July 2001.
- [6] Tangirala, V.E., Hinckley, K.M., Chapin, D.M., Dean, A.J.: USPTO20070180814 (2007).
- [7] Tequesta, W.W., Jupiter, B.F.R.B.: EP1903206 (2008).
- [8] Reid RC, Prausnitz JM, Sherwood TK. The properties of gases and liquids. New York: Mc-Graw Hill Book Company 1977.
- [9] Sengers J. Critical behaviour in fluids. London: Mc-Graw Hill Book Company 1977.
- [10] Kuo KK. Principle of combustion. New York: John Wiley and Sons 1986.
- [11] Minotti A, Bruno C. Sub-trans and supercritical properties for LO₂-CH₄ at 15MPa. J Thermophys Heat Transfer 2007; 21(4): 796-810.
- [12] Minotti A. Modelling of O₂/CH₄ Liquid rocket engine injector combustion at subcritical and supercritical conditions. PhD Thesis, University of Rome La Sapienza, Department of Mechanics and Aeronautics 2007.
- [13] Chehroudi B, Talley D, Coy E. *Initial growth rate and visual characteristic of a round jet into a sub-supercritical environment of relevance to rocket, gas turbine and diesel engines*. 37th AIAA Aerospace Sciences Meeting and Exhibit, AIAA, 99-0206, Reno, NV 1999.
- [14] Chehroudi B, Talley D, Coy E. Fractal geometry and growth rate changes of cryogenic jets near the critical point. Atom Sprays 2004; 14(1): 81-91.
- [15] Mayer W, Tamura H. Propellant injection in a liquid oxygen/gaseous hydrogen rocket engine. J Propul Power 1996; 12(6): 1137-47.
- [16] Mayer W, Schik A, Schweitzer C, Schaffer M. Injection and mixing process in high pressure LO₂/GH₂ rocket combustors. J Propul Power 2000; 16: 823-28.
- [17] Mayer W, Schik A, Vielle B, et al. Atomization and breakup of cryogenic propellant under high pressure subcritical and supercritical conditions. J Propul Power 1998; 14: 835-42.
- [18] Mayer W, Ivancic B, Schik A, Hornung U. Propellant atomization in LO₂/GH₂ rocket engines. J Propul Power 2001; 17: 794-99.
- [19] Oefelein J, Yang V. *Simulation and analysis of supercritical multiphase combustion processes*. 32nd Joint Propulsion Conference and Exhibit, AIAA-1996-2880, Lake Buena Vista, FL July 1996.
- [20] Oefelein J. Simulation and analysis of supercritical multiphase combustion processes at high pressure. Ph.D. thesis, The Pennsylvania State University, Department of Mechanical Engineering 1997.
- [21] Oefelein J, Yang V. Modelling high pressure mixing and combustion processes in liquid rocket engines. J Propul Power 1998; 14: 843-57.
- [22] Zong N, Meng H, Hsieh S, Yang V. A numerical study of cryogenic fluid injection and mixing under supercritical conditions. Phys Fluids 2004; 16: 4248-61.
- [23] Yang V, Zong N. Near field flow and flame dynamics of LO₂/methane shear coaxial injector under supercritical conditions. Proc Combust Inst 2007; 31 (2): 2309-17.
- [24] Bellan J. Theory, modelling and analysis of turbulent supercritical mixing. Comb Sci Technol 2006; 178: 253-81.
- [25] O'Kongo N, Harstad K, Bellan J. Direct numerical simulation of LO_x-H₂ temporal mixing layers under supercritical conditions. AIAA J 2002; 40: 914-26.
- [26] Lux J, Suslov D, Bechle M, Oschwald M, Haidn O. *Investigation of sub- and supercritical LO₂/Methane injection using optical diagnostic*. 42nd AIAA Joint Propulsion Conference & Exhibit, Sacramento, California 2006-5077, July 2006.
- [27] Zong N, Ribert G, Yang V. *Supercritical combustion of liquid oxygen and methane stabilized by a splitter plate*. 45th AIAA Aerospace Sciences Meeting & Exhibit, AIAA 2006-5077, Reno January 2007.
- [28] Zong N, Yang V. *Supercritical LO₂/Methane flame stabilization and dynamics of a shear coaxial injector*. 44th AIAA Aerospace Sciences Meeting & Exhibit. AIAA 2006-760, Reno Nevada, January 2006.
- [29] Ruiz A. *Large eddy simulation of transcritical round jets*. 3rd EUCASS, Versailles Conference centre, Versailles, Paris, France 2009.
- [30] De Giorgi MG. Real fuel modelling of supercritical reacting flows in liquid rocket engine. 3rd EUCASS, Versailles Conference centre. Paris, France: Versailles 2009.
- [31] <http://webbook.nist.gov/>
- [32] Lee BI, Kesler MG. A generalized thermodynamic correlation based on three-parameter corresponding states. AIChE J 1975; 21(3): 510-27.
- [33] Soave G. Study of drop coalescence behavior for liquid-liquid extraction operation. Chem Eng Sci 1972; 27: 1503-07.
- [34] Redlich Robert C, Kwong JNS. Critical phenomena in binary liquid systems. Chem Rev 1949; 44 (1): 233-44.
- [35] Peng Ding-Yu, Robinson DB. A new two constant equation of state. Ind Eng Chem Fundam 1976; 15: 59-64.
- [36] Congiunti A, Bruno C, Giacomazzi E. Supercritical combustion properties. 41st Aerospace Science Meeting and Exhibition. AIAA 2003-0478, Reno, Nevada January 2003.
- [37] Harstad KG, Miller RS, Bellan J. Efficient high pressure state equation. AIChE J 1997; 43(6): 1605-10.
- [38] Chung TH, Ajlan M, Lee LL, Starling KE. Generalized multiparameter corresponding state correlation for polyatomic, polar fluid transport properties. Ind Chem Eng Res 1988; 27: 671-79.
- [39] Ely JF, Hanley HJM. Thermal conductivity of pure fluids and mixtures. Ind Eng Chem Fundam 1981; 22(4): 90-97.
- [40] Mayer W, Telaar J, Branana R, Schneider G, Hussong J. Characterization of cryogenic injection at supercritical pressure. J Propul Power 2003; 19(3): 342-55.
- [41] Haidn OJ. *H₂-O₂ supercritical combustion modeling using a CFD code*. Proceedings of the 2nd international workshop on rocket combustion modelling, DLR, Lampoldhausen, Germany 2001; 25-27.
- [42] Rehab H, Villermaux E, Hopfinger E. Flow regimes of large velocity ratio coaxial jets. J Fluid Mech 1998; 345: 357-81.
- [43] Villermaux E. Mixing and spray formation in coaxial jets. J Propul Power 1998; 14(5): 807-17.
- [44] Ierardo N, Congiunti A. *Mixing and combustion in supercritical O₂/CH₄ liquid rocket injectors*. 42nd AIAA meeting, AIAA 2004-1163, Reno, January 2004.
- [45] Gordon S, McBride BJ, Zeleznik FJ. Computer program for calculation of complex chemical equilibrium composition and applications, supplement I-Transport Properties. NASA TM-86885 1984.
- [46] Gordon S, McBride BJ. Computer program for calculating and fitting thermodynamic functions. NASA RP-1271 1992.
- [47] Gordon S, McBride BJ, Reno MA. Thermodynamic data for fifty reference elements. NASA TP-3287 1993.
- [48] Gordon S, McBride BJ, Reno MA. Coefficients for calculating thermodynamic and transport properties of individual species. NASA TM-4513 1993.
- [49] FluentTM. Software. Ver. 6.2.16 User's Guide, Ch. 8.4.3, Lebanon, NH USA: Fluent, Inc., 2005.
- [50] FluentTM. Software. Ver. 6.2.16 User's Guide, Ch. 8.5.3, Lebanon, NH USA: Fluent, Inc., 2005.
- [51] Giacomazzi E. Modelling and simulation of turbulent combustion. PhD Thesis, University of Rome La Sapienza, Department of Mechanics and Aeronautics 1999.
- [52] Gran IR, Magnussen BF. A numerical study of a Bluff-Body stabilized diffusion flame. Part 2. Influence of combustion modelling and finite-rate chemistry. Comb Sci Technol 1996; 119: 1-6.

- [53] Magnussen BF. *On the structure of turbulence and a generalized eddy dissipation concept for chemical reaction in turbulent flow*. 19th Aerospace Science Meeting, AIAA, St. Louis, Mo., 1981; 42: 1-8.
- [54] Magnussen BF, Hjertager BH. *On mathematical modelling of turbulent combustion with special emphasis on soot formation and combustion*. 16th Symp. on Comb, the Combustion Institute, Pittsburg, 1977; 719-29.
- [55] Spalding DB. *Mixing and chemical reaction in steady confined turbulent flames*. 13th Symp On Comb, The Combustion Institute, Pittsburgh, 1971; 649-57.
- [56] Westbrook CK, Dryer FL. Simplified reaction mechanisms for the oxidation of hydrocarbon fuels and flames. *Comb Sci Technol* 1981; 27(1-2): 31-43.
- [57] CHEMKIN Software, Ver. 3.7. Comprehensive chemical kinetics. USA, Elsevier's Science & Technology publishing 2004.
- [58] Spalart RP. Direct simulation of a turbulent boundary layer up to $Re=1410$. *J Fluid Mech* 1988; 187: 61-98.
- [59] Kim J, Moin P, Moser R. Turbulence statistics in fully developed channel flow at low Reynolds number. *J Fluid Mech* 1987; 177: 133-66.

Received: July 15, 2009

Revised: September 9, 2009

Accepted: October 7, 2009

© Minotti and Bruno; Licensee *Bentham Open*.

This is an open access article licensed under the terms of the Creative Commons Attribution Non-Commercial License (<http://creativecommons.org/licenses/by-nc/3.0/>) which permits unrestricted, non-commercial use, distribution and reproduction in any medium, provided the work is properly cited.